Applied Energy 208 (2017) 766–781

Contents lists available at ScienceDirect

Applied Energy

journal homepage: www.elsevier.com/locate/apenergy

Real-time optimization of a chilled water plant with parallel chillers based on extremum seeking control

Baojie Mu[a], Yaoyu Li[b,*], John M. House[c], Timothy I. Salsbury[c]

[a] Research & Engineering Center, Whirlpool Corporation, Benton Harbor, MI 49022, USA
[b] Department of Mechanical Engineering, The University of Texas at Dallas, Richardson, TX 75080, USA
[c] Building Efficiency Research Group, Johnson Controls Inc., Milwaukee, WI 53201, USA

HIGHLIGHTS

- Proposes a model-free optimization scheme for parallel-chiller plant with multivariable ESC.
- Penalty-function multivariable ESC is used to avoid integral windup due to actuation saturation.
- The chiller sequencing control logic is based on ESC inherent control signals.
- Validated with simulations on a Modelica based model of a two-chiller plant.
- Simulation results show good steady-state performance and reasonable transient performance.

ARTICLE INFO

Keywords:
Chiller plant optimization
Chiller sequencing
Multivariable extremum seeking control
Penalty function
Modelica

ABSTRACT

Chilled water plants with multiple chillers are commonly used to provide cooling in large commercial buildings. Optimization offers a significant opportunity for improving the energy efficiency of such plants. Model based approaches used for control and optimization require accurate models, which can be difficult and/or expensive to obtain in practice due to large variations in equipment characteristics and operating conditions. In this paper, a model-free optimization strategy based on multivariate Extremum Seeking Control (ESC) with penalty terms is proposed for maximizing the energy efficiency of a chilled-water plant with parallel chillers. The feedback to ESC is the total power consumption of the plant consisting of chiller compressors, cooling tower fan, and condenser water pumps, in combination with penalty terms for input-saturation. The control inputs include the cooling tower fan airflow, condenser water flows and evaporator leaving chilled-water temperature setpoint. A band-pass filter array, instead of the high-pass filter in the standard ESC, is adopted to reduce the coupling among the input channels. The proposed strategy is evaluated with simulation study using a Modelica based dynamic simulation model of a chilled-water plant with two parallel chillers. Six cases are presented that demonstrate real-time optimization capability of ESC for this application.

1. Introduction

In 2010, the United States consumed 97.8 Quads (1 Quad = 10^{15} BTU) of primary energy, with 19% of this consumption attributed to commercial buildings [1]. Space cooling accounts for 10–13% of energy consumption in commercial buildings [2], and in large commercial buildings, a significant fraction of this consumption is by the chilled water plant, where compressors, pumps and fans work to deliver cold water that is used for cooling. Thus, improvements in the energy efficiency of chilled water plants have the potential to yield large reductions in primary energy consumption. This realization has resulted in numerous studies in the literature reporting efforts aimed at developing control strategies that optimize the operating performance of chilled water plants. These studies can be divided into three categories, namely: rule-based control, model-based control, and model-free control.

Rule-based control approaches typically employ an exhaustive search technique requiring extensive simulations and/or experiments to determine settings for manipulated variables that optimize system operation. Studies in the literature have used manufacturer performance data and field measurements with analytical and/or regression models of plant performance to optimize condenser water flow and tower fan speed [3,4]. Hydeman and Zhou [5] propose an optimal chiller-sequencing strategy using a parametric model based on simulation data.

* Corresponding author.
E-mail addresses: baojie_mu@whirlpool.com (B. Mu), yaoyu.li@utdallas.edu (Y. Li), John.M.House@jci.com (J.M. House), Timothy.I.Salsbury@jci.com (T.I. Salsbury).

http://dx.doi.org/10.1016/j.apenergy.2017.09.072
Received 23 October 2016; Received in revised form 9 September 2017; Accepted 11 September 2017
Available online 24 September 2017

Nomenclature

A	heat transfer area (m^2)
a_i	the i-th channel dither magnitude
AmRH	ambient relative humidity (%RH)
AmT	ambient dry bulb temperature (°C)
CHDP	differential pressure for the primary chilled-water loop (kPa)
CHF	chilled water pump flow rate (kg/s)
CHi	chiller #i, $i = 1, \dots, N$
CHiSH	chiller #i superheat measurement (°C)
CHiTXVO	chiller #i thermal expansion valve opening (%)
CHP	chilled water pump
CHVO	chilled water valve opening (%)
CHWST	chilled water supply temperature (°C)
COMP	compressor speed (Hz)
CTA	cooling tower air flow (kg/s)
CTF	cooling tower fan
CWF	condenser water flow rate (kg/s)
CWP	condenser water pump
d_h	hydraulic diameter (m)
ESCj	channel #j of ESC controller, $j = 1, \dots, M$.
ESCjg	gradient measurement of channel #j of ESC controller
ESCjs	command signal of channel #j of ESC controller
$F_{BP}(s)$	transfer function of band-pass filter
$F_{IN}(s)$	transfer function of input dynamics
$F_{LP}(s)$	transfer function of low-pass filter
$F_{HP}(s)$	transfer function of high-pass filter
$F_O(s)$	transfer function of output dynamics
$f(\cdot, \cdot)$	time-varying performance map
h	specific enthalpy (kJ/kg)
K	ESC loop gain vector
L	augmented cost
L_p	sum of the chiller plant total power and saturation induced penalty terms
$\dot{m}$	mass flow rate (kg/s)
$M(t)$	demodulation signal
Nu	Nusselt number
P_t	total power of chiller compressors, cooling tower fan and chilled water pumps (kW)
Pr	Prandtl number
Q	heat transfer (J)
Re	Reynolds number
RmQ	room (zone) internal cooling load (kW)
RmT	room (zone) temperature measurement (°C)
$S(t)$	dither signal
SAT	supply air temperature measurement (°C)
SH	superheat (°C)
T	temperature (°C)
V	volume (m^3)
VAVO	VAV box damper opening (%)
x^*	flow stream quality
y	plant output
y_p	penalty cost
u	control input vector of ESC

Greek symbols

α	heat transfer coefficient (W/m^2 K)
γ	penalty weight
ζ	damping ratio of band-pass filter
η	efficiency
λ	thermal conductivity (W/m K)
ρ	density (kg/m^3)
ω_i	the ith channel dither frequency
Ω_{COMP}	compressor speed
ψ_i	phase angle between dither and demodulation signals for the ith channel

Although the reported work on rule-based control [6] has demonstrated good performance for specific systems under tested conditions, significant variation in performance is observed in practice due to factors such as nonlinear behavior of equipment and equipment degradation. These realities necessitate adjustments to the chiller water plant operating rules over the life cycle of the equipment and this, in turn, increases the cost of operation and maintenance and limits the ultimate benefit of rule-based control.

Numerous studies in the literature report model-based control approaches for chiller plant optimization. Using a semi-empirical chiller performance model [7], Powell et al. [8] apply a mixed-integer nonlinear programming technique to optimize the chilled water plant for a campus cooling network. Using a simplified load-dependent chiller model, Olson and Liebman [9] apply a sequential quadratic programing (SQP) scheme to minimize plant power consumption. Kusiak et al. [10] apply eight data-mining algorithms to model the nonlinear behavior of the chiller plant performance from experimental data. The resultant model is used to minimize plant energy consumption by regulating the supply air temperature setpoint and static pressure setpoint of the air-handling unit (AHU) served by the chiller plant. Huang et al. [11] propose a heuristic optimization approach to chiller plant optimization and control. Recently, model predictive control (MPC) has attracted significant research effort in the area of building control. MPC can handle input and state constraints as well as future information in solving the associated real-time optimization problem. For a central chilled-water plant with multiple chillers and thermal energy storage, Deng et al. [12] apply MPC to thermodynamic models derived for this plant, and a receding-horizon optimal scheduling solution is obtained to minimize the total energy consumption. Based on a linear parameter-varying model for a chiller plant, Zhu et al. [13] use MPC to optimize the setpoint for the chilled-water supply temperature. Studies reported in the literature demonstrate the potential savings from model-based control; however, the performance of these approaches relies on the accuracy of the plant models. This limitation can be a significant barrier to widespread deployment.

Model-free control based chiller-plant optimization approaches are also prevalent in the literature, with most of the methods being based on machine learning and artificial intelligence, such as neural networks, genetic algorithms (GA), and particle swarm optimization (PSO). Chow et al. [14] integrate a neural network and GA to optimize the total power consumption for an absorption chiller plant. Chang et al. [15] and Ma and Wang [16] report studies where GA schemes are used for chiller plant optimization. Lee and Lin [17] apply a PSO based approach to reduce the energy consumption of a multi-chiller system by regulating the part load ratio (PLO) for each chiller. Ardakani et al. [18] also apply PSO to optimize the PLO of a chiller plant and demonstrate the convergence speed of the PSO approach is faster than conventional GA schemes. The primary limitation of GA and PSO approaches is that they require the availability of a sufficiently rich historic data set, and convergence behavior and solutions can be random.

As a model-free approach, Extremum Seeking Control (ESC) [19] has emerged as a promising real-time optimization solution for energy efficient operation of heating, ventilating and air-conditioning (HVAC) applications. ESC estimates the gradient online based on a dither-demodulation scheme, and thus the search process is robust to external disturbance and process variation. ESC responds to actual plant behavior in real time, and thus its convergence rate is typically faster than machine learning methods. Li et al. [20] study and apply an ESC

strategy for optimization of air-side economizer operation in an AHU. Experimental validation of the strategy is demonstrated in [21] for two types of AHUs, one having a direct-expansion cooling coil and the other a chilled water cooling coil. Burns and Laughman [22], Xiao et al. [23] and Dong et al. [24] apply ESC to optimize the energy efficiency of mini-split heat pumps by manipulating the evaporator fan speed, condenser fan speed, suction superheat setpoint, and combinations of these input variables. Hu et al. [25] report an application of ESC to ground source heat pumps. Sane et al. [26] propose a single-input ESC to minimize the total power consumption of a chilled water plant by manipulating the condenser water supply temperature setpoint. For minimizing the power consumption of a chiller-tower plant, Li et al. [27] control the tower fan speed with ESC based on the feedback of total power. Mu et al. [28] compare dither ESC with switching ESC, sliding mode ESC, and simultaneous perturbation stochastic approximation (SPSA) on a chiller plant model. Later, Mu et al. [29] further the work in [27] to multivariable ESC that optimizes the tower air flow and condenser water flow simultaneously.

This paper describes an optimization strategy for a chilled-water plant with two parallel chillers and a single cooling tower based on a multivariable gradient-based ESC framework. The feedback for ESC is a performance index consisting of the total power consumption of the equipment in the chilled-water plant plus penalty terms due to input saturation. The manipulated inputs include the airflow rate of the cooling tower fan, the condenser water flow rates, and the chilled water supply temperature setpoint. In order to reduce the coupling among the input channels, a band-pass filter array is used, as opposed to the high-pass filter used in the standard ESC configuration. With a penalty-function based anti-windup scheme, integral windup due to input saturation can be avoided. A comprehensive simulation study is conducted to evaluate the strategy using a Modelica based chilled-water plant with two parallel chillers.

The paper builds on the work reported by the authors in two conference papers [30,31] by describing the plant model used for the simulations, presenting a more comprehensive set of simulation results, and including global optimization results obtained offline using a genetic algorithm and Simplex method that verify the ESC results. The new simulation results include a case with input variable saturation and a case where a fault results in plant performance degradation. The penalty-function based anti-windup capability allows ESC to overcome the possible interruption of optimum seeking process due to actuator saturation for one or multiple input channels. Performance degradation due to faults are a reality of chilled-water plants and the results presented highlight the real-time optimization benefit of ESC.

The remainder of this paper is structured as follows. The penalty-function based multi-variable ESC is outlined in Section 2, and the ESC based chiller-plant optimization strategy is presented in Section 3. A Modelica based dynamic simulation model for components of the chilled-water plant is presented in Section 4. The controller design is then presented, followed by a simulation study with ESC applied to different scenarios. Finally, conclusions of this work are presented.

2. Multi-variable ESC with penalty-function based anti-windup

ESC is a model-independent real-time optimization strategy [32–34] that aims to search for the inputs to a nonlinear dynamic plant that minimize a specific performance index, i.e. $u^*(t) = \arg\min_u f(u,t)$, where $u = [u_1 \ \cdots \ u_n]^T$ is the vector of control inputs, and $f(u,t)$: $\mathbb{R}^n \times \mathbb{R}^1 \rightarrow \mathbb{R}^1$ is the performance index with a unique minimum within the domain of inputs. For simplicity, f is assumed to be convex and thus contain a global minimum. As shown in Fig. 1, based on the Wiener-Hammerstein approximation, the input and output dynamics can be simplified as linear time-invariant (LTI) systems $F_{IN}(s)$ and $F_O(s)$, respectively, both with unity gain. The gradient is estimated using a dither signal $S(t) = [S_1(t) \ \cdots \ S_n(t)]^T$ with $S_i(t) = a_i \sin(\omega_i t)$ $(i = 1, \ldots, n)$, demodulation signal $M(t) = [M_1(t) \ \cdots \ M_n(t)]^T$ with $M_i(t) = \frac{2}{a_i}\sin(\omega_i t + \psi_i)$, high-pass (HP) and low-pass (LP) filters. After demodulation, the gradient-proportional signal is passed through LP and then integrated with gain $K = [K_1 \ \cdots \ K_n]^T$ to produce the control input. Optimality will be obtained if asymptotic stability can be achieved for the integral control of the estimated gradient.

An issue with using just one high-pass filter is that the demodulation process may yield a number of low frequency components that lead to undesirable oscillations in the system inputs and output unless low-pass filters with very low cut-off frequencies are used. The undesirable consequence of the low bandwidth is *very slow convergence*. As shown in Fig. 2, the authors [30] consider the replacement of the high-pass filter by a band-pass (BP) filter array $F_{BP}(s) = [F_{BP,1}(s),\ldots,F_{BP,n}(s)]^T$ with $F_{BP,i}(s) = \frac{2\zeta\omega_i s}{s^2 + 2\zeta\omega_i s + \omega_i^2}$. This modification makes the demodulated signals contain isolated harmonics at their respective dither frequency, and thus achieve significant decoupling for the input channels. For each input channel, an anti-notch BP filter is chosen due to its good quality factor and zero-phase response at the respective dither frequency. Also, a higher bandwidth is made possible for the low-pass filter design, and the convergence can be accelerated. The phase angle ψ_i should be chosen such that $\theta_i = \psi_i + \angle F_{IN,i}(j\omega_i) = 0$, and at least within $\left(-\frac{\pi}{2}, \frac{\pi}{2}\right)$.

Under the presence of input saturation, integrator windup could lead to undesirable performance for the extremum seeking process, e.g. under the change of operating conditions [20]. In this study, the penalty-function based anti-windup ESC framework in [35] is extended to a multivariable setting for the chilled-water plant. As shown in Fig. 2, the portions of inputs outside the input limits are penalized as additional cost terms in the performance index. The augmented objective function is thus $L = y + y_p$, where $y_p = \sum_{i=1}^{n} \phi_i(\cdot)$, $\phi_i(\cdot) = \frac{1}{2}\gamma_i[sat(u_i) - u_i]^2$, and γ_i is the weight of the ith penalty term. The saturation (or limiter) operation is defined as

$$sat(u) = u_{sat} \triangleq \begin{cases} u_{\max}, & u \geqslant u_{\max} \\ u, & u_{\min} < u < u_{\max} \\ u_{\min}, & u \leqslant u_{\min} \end{cases} \tag{1}$$

where u denotes a general input, and subscripts 'min' and 'max' stand for the minimum and maximum value, respectively. Compared to the conventional ESC as shown in Fig. 1, the penalty-function based multivariable ESC involves additional parameters γ_i for the penalty terms against saturation. The penalty-augmented cost function can then be expanded as

$$L = y + y_p = f(u) + \frac{1}{2}[sat(u^m) - u^m]^T \gamma [sat(u^m) - u^m] \tag{2}$$

where $u^m = [u_1 \ \cdots \ u_m]^T$ is a vector of inputs that are under saturation $(1 \leqslant m \leqslant n,\ m \in \mathrm{Z})$, and $\gamma = diag(\gamma_1 \ \cdots \ \gamma_m)$ is the weight matrix.

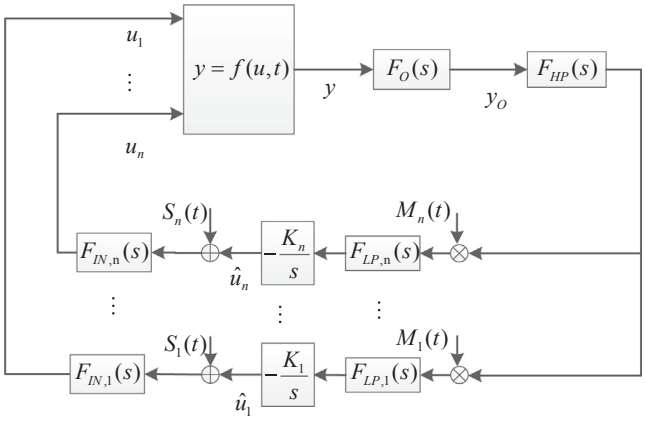

Fig. 1. Block diagram of multivariate ESC with HP filter.

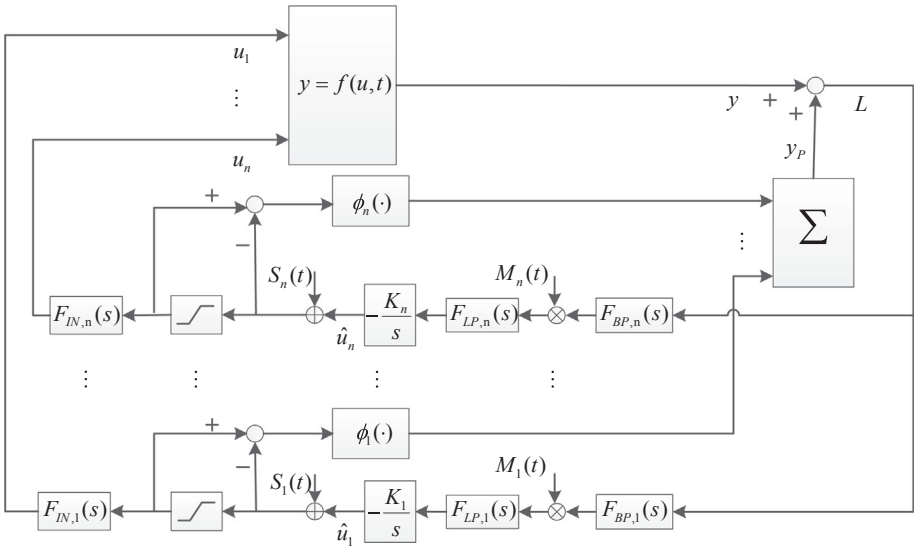

Fig. 2. Penalty-function based anti-windup multivariate ESC with BP filter array.

3. ESC based optimization for chilled-water plant with parallel chillers

Fig. 3 is a schematic diagram of a chilled water plant with two parallel chillers serving a single air-handling unit (AHU). This is a common configuration for a chilled water plant, although many variations exist, including configurations with the chillers arranged in series. Furthermore, a plant with multiple chillers would typically serve the load of multiple AHUs. With this study being an initial proof-of-concept evaluation for the proposed model-free approach, the key requirements of the chilled-water plant configuration and the associated simulation model is that they be representative of an actual chiller plant. Both the configuration and model satisfy this requirement.

Chillers commonly use a vapor compression refrigeration cycle to produce chilled water, which is pumped through the chilled water distribution loop to one or more AHUs and used to cool air that is distributed to achieve space cooling. The chilled water is then returned at an elevated temperature. Heat absorbed from the returning water by refrigerant in the evaporator of the chiller is rejected to a separate water loop in the condenser. Heat absorbed by the condenser water is rejected to the ambient via evaporative cooling in the cooling tower. A chilled-water plant includes all components and systems in Fig. 3 except the AHU and associated air distribution components.

In this study, each chiller has a variable-capacity compressor (COMP) that is used to regulate the chilled water supply temperature (CHWST), a condenser water pump (CWP) that is used to adjust the condenser water flow rate (CWF), and a chilled water pump (CHP) that is used to control the pressure in the chilled water loop to ensure an adequate flow rate of chilled water to the AHU cooling coil. Without loss of generality, the condensing water of all chillers is assumed to be cooled with a single cooling tower, and the cooling tower airflow rate (CTA) is adjusted by a cooling tower fan (CTF).

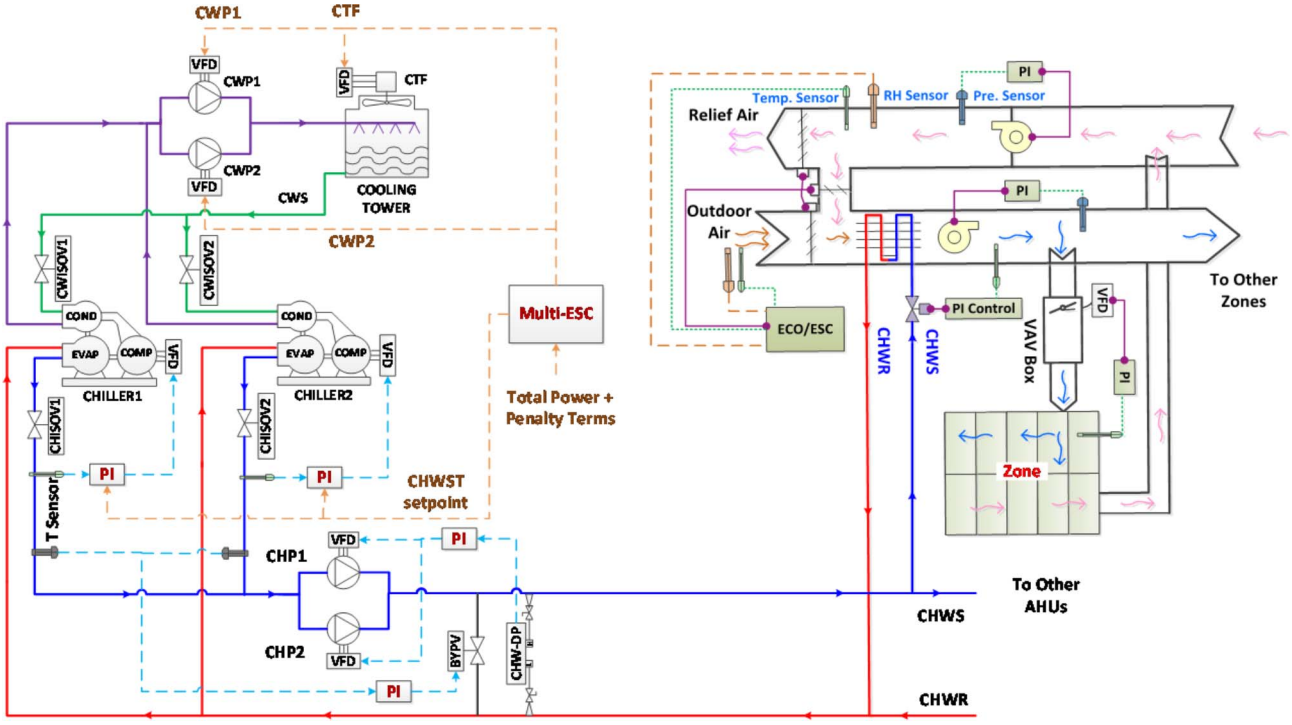

Fig. 3. Schematic diagram of the chilled water plant with two chillers in parallel.

The objective of chilled-water plant optimization is to minimize the total power consumption, provided that the AHU supply air temperature (SAT), suction superheat (SH) as well as other internal-loop PI controls are regulated to their respective setpoints. The optimization problem thus becomes

$$\min P_t(t) = \min\{P_{CTF}(t) + \sum_{i=1}^{n} \delta_i[P_{COMP,i}(t) + P_{CWP,i}(t) + P_{CHP,i}(t)]\} \tag{3a}$$

subject to:

$$\dot{m}_{CTA,min} \leqslant \dot{m}_{CTA} \leqslant \dot{m}_{CTA,\max} \tag{3b}$$

$$\dot{m}_{CWF,i,min} \leqslant \dot{m}_{CWF,i} \leqslant \dot{m}_{CWF,i,\max} \tag{3c}$$

$$\dot{m}_{CHF,i,min} \leqslant \dot{m}_{CHF,i} \leqslant \dot{m}_{CHF,i,\max} \tag{3d}$$

$$\Omega_{COMP,i,\min} \leqslant \Omega_{COMP,i} \leqslant \Omega_{COMP,i,\max} \tag{3e}$$

$$T_{SAT,i,\min} \leqslant T_{SAT,i} \leqslant T_{SAT,i,\max} \tag{3f}$$

$$T_{SH,i,\min} \leqslant T_{SH,i} \leqslant T_{SH,i,\max} \tag{3g}$$

where

$$\delta_i = \begin{cases} 1 & \text{if chiller } i \text{ is ON} \\ 0 & \text{if chiller } i \text{ is OFF} \end{cases} \tag{4}$$

denotes whether the ith chiller is enabled to operate or disabled.To handle input constraints associated with plant operation, the objective function is augmented with a penalty term related to input saturation, i.e.

$$L_p(t) = P_t(t) + y_p(t) \tag{5}$$

with respect to the regulation of $\dot{m}_{CTA}$, $\dot{m}_{CWF}$ and the CHWST setpoint regulated by the compressor speed. $y_p(t)$ is a quadratic penalty function defined as

$$\begin{aligned} y_p(t) = \sum_{i=1}^{n} \phi_i(\cdot) = {} & \frac{1}{2}\gamma_{CTA}(\dot{m}_{CTA}-\dot{m}_{CTA,sat})^2 + \frac{1}{2}\gamma_{CWF,i}(\dot{m}_{CWF,i}-\dot{m}_{CWF,i,sat})^2 \\ & + \frac{1}{2}\gamma_{COMP,i}(\Omega_{COMP,i}-\Omega_{COMP,i,sat})^2 + \frac{1}{2}\gamma_{CHF,i}(\dot{m}_{CHF,i}-\dot{m}_{CHF,i,sat})^2 \\ & + \frac{1}{2}\gamma_{SH,i}(T_{SH,i}-T_{SH,i,sat})^2 + \frac{1}{2}\gamma_{SAT,i}(T_{SAT,i}-T_{SAT,i,sat})^2 \end{aligned} \tag{6}$$

where subscript '*sat*' denotes the output of the limiter. γ_{CTA}, $\gamma_{CWF,i}$, γ_{COMP}, $\gamma_{CHF,i}$, $\gamma_{SH,i}$, and $\gamma_{SAT,i}$ denote the weights of corresponding penalty terms, respectively.

The controls inputs for ESC for a chilled water plant with multiple chillers are selected as: the cooling tower air flow rate, the water flow rate through each condenser water pump, and the CHWST setpoint of each chiller. As a reasonable simplification, all chillers are assumed to have the same CHWST setpoint.

A model-free optimal chilled water plant control strategy using the penalty-function based multivariate anti-windup ESC is proposed here. The strategy aims to minimize the total power consumption of the chilled-water plant in real time. The cooling load that the chilled-water plant must offset is time varying and different sequencing strategies can be used to turn on and off chillers and associated pumps in order to match the plant capacity to this load. As equipment turns on and off, the ESC manipulated variables change. In this study it is assumed that the two chillers are identical in capacity and the sequencing strategy is to exhaust the capacity of the current operating chiller before enabling the operation of the next chiller, a common practice in chiller plant operation. Details of the sequencing strategy are provided in the description of sequencing Scheme-I in [30]. To achieve a smooth transition during startup/shutdown of equipment, bumpless transfer based on the conditional integration (CI) scheme [36] is used.

Table 1
ESC design parameters for one-chiller ESC.

Parameter	ESC1 (CTA)	ESC2 (CWF)	ESC3 (CHWST)
Dither frequency (rad/s)	0.005	0.0038	0.0013
Dither amplitude	3 kg/s	3 kg/s	0.5 °C
Demodulation amplitude	2/3 kg/s	2/3 kg/s	4 °C
Demodulation phase (rad)	0.92	0.97	1.01
ω_{BPL} (rad/s)	0.0045	0.0034	0.0012
ω_{BPH} (rad/s)	0.0055	0.0042	0.0014
ω_{LP} (rad/s)	0.0025	0.0019	0.00615
Integrator gain	0.0015	0.00048	0.0004
Input range	[5, 55] kg/s	[5, 40] kg/s	[2, 11] °C

4. Dynamic simulation model of chilled water plant

A simulation study is performed to evaluate the proposed strategy of chilled water plant optimization. A dynamic simulation model is developed for the plant shown in Fig. 3 using Dymola 2015 [37] using the TIL Library 3.1 [38]. The chiller model consisting of a compressor, condenser, thermal expansion valve (TXV), and evaporator is developed using TIL Library 3.1.

The variable-speed compressor model is based on the following efficiency based equations:

$$\eta_{vol} = \frac{\dot{m}_{rfg}}{V\Omega\rho} \tag{7a}$$

$$\eta_{is} = \frac{h_{d,is}-h_s}{h_d-h_s} \tag{7b}$$

$$\eta_{eff,is} = \frac{\dot{m}_{rfg}(h_{d,is}-h_s)}{2\pi\tau\Omega} \tag{7c}$$

where Ω is the compressor speed. η_{vol}, η_{is} and $\eta_{eff,is}$ are the volumetric efficiency, isentropic efficiency, and effective isentropic efficiency, respectively. $\dot{m}_{rfg}$ is the mass flow rate of refrigerant, V is the volume of compressor displacement, ρ is the refrigerant density, τ is the driving torque, and h denotes the enthalpy. Subscripts 'd' and 's' denote the discharge and suction sides of the compressor, respectively, and 'is' refers to the isentropic condition.

The evaporator and condenser are modeled using a parallel flow heat exchanger module from the TIL Library. This module is based on the finite volume method, where for each cell in the control volume, the heat flow rate is governed by

$$\dot{Q} = \alpha A(T_w-T) \tag{8}$$

where α is the heat transfer coefficient, A is the heat transfer area, T_w and T are the wall and cell temperature, respectively. For single-phase flow at the refrigerant side,

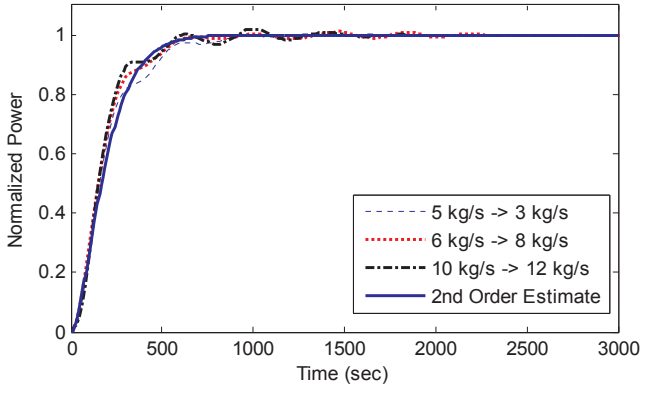

Fig. 4. Step responses of CTA input channel and input dynamics estimate.

$$\alpha = \frac{Nu\lambda}{d_h} \tag{9}$$

where Nu is the Nusselt number, λ is the thermal conductivity, and d_h is the hydraulic diameter. For the two-phase flow,

$$\alpha = 0.023 Re^{0.8} Pr^{0.4} \left[(1-x^*)^{0.8} + \frac{3.8(1-x^*)^{0.04} x^{*0.76}}{Pr^{0.38}} \right] \tag{10}$$

where Pr is the Prandtl number, Re is the Reynolds number, and x^* is the flow stream quality, which is defined as

$$x^* = \frac{\dot{m}_g}{\dot{m}} \tag{11}$$

where subscript g refers to the gas phase [39].

The expansion valve is modeled as an isenthalpic process that does not have transient mass storage [38,39]. The mass flow rate and the pressure difference across the valve follow a quadratic relationship. The effective area of this valve is used for regulating the suction superheat of the chiller.

The cooling tower model is based on the model described in [27] and is updated to be compatible with Dymola 2015. The AHU model is developed from components in the TIL Library 3.1 [38] and consists of three interlocked dampers to control the intake of outdoor air, one cooling coil, two duct fans, and one VAV box for controlling airflow into the zone. The AHU model is used to provide a representative load on the chiller-water plant and its power consumption is not included in the optimization strategy. Thus, a detailed description of the model is omitted in the interest of brevity.

Detailed parameter specifications of the chiller components are given in Appendix A. The maximum capacity for each chiller is 507 kW according to the Application Rating Conditions defined by AHRI Standard 550/590 [40].

5. Simulation study

The proposed strategy is tested using the Modelica simulation model described in the previous section. The following regulation control loops are implemented with PI controllers:

(1) The thermal expansion valve opening (TXVO) of each chiller regulates superheat (SH) at the inlet to the compressor to 5 °C. The range of this setpoint is 3–7 °C.
(2) The compressor speed of each chiller regulates the CHWST to the setpoint determined by ESC. The range of this setpoint is 2–11 °C.
(3) The chilled water pumps (CHP) regulate the differential pressure for the primary chilled water loop (CHDP) to 300 kPa. The range of this setpoint is 280–320 kPa.
(4) The AHU chilled water valve opening (CHVO) is regulated to maintain the supply air temperature at 13 °C. The range of this setpoint is 11–15 °C.
(5) The AHU supply-air fan is regulated to maintain the pressure in the supply-air duct at 103.1 kPa. The range of this setpoint is 101.1–105.1 kPa.
(6) The VAV box damper opening (VAVO) regulates the room temperature (RmT) at 25 °C.

As noted previously, normal operation of a chilled water plant involves turning chillers and associated pumps on and off to satisfy the time-varying load from the AHU(s). The operational specifications for compressors, condenser water pumps and the cooling tower fan during startup and shutdown are given as follows:

(1) The capacity of a compressor is defined by the speed (Hz). The maximum speed of the compressor is 100 Hz while the nominal minimum speed is defined as 30 Hz. To start a compressor during chiller startup, its speed is increased from 0 Hz to the nominal minimum speed at a rate of 1.5 Hz/s.
(2) To turn off the compressor during chiller shutdown, its speed is decreased from its current value to 0 Hz at a rate of 1.5 Hz/s.
(3) The condenser water pump and chilled water pump of a chiller that is starting are initialized from zero flow and increased to preset values during startup. During shutdown, a pump decreases the flow from its current value to zero. The preset values can be determined in different ways, for example: (i) the midpoint of the operational range for the pump; or (ii) some value derived from a load estimate based on some assumed model knowledge.

The ESC design starts with dither frequency selection, which is based on the input dynamics estimated with open-loop step tests under ambient conditions of 27 °C dry-bulb temperature and 60 percent relative humidity (%RH), and internal heat gain in the zone of 250 kW. At this load, a single chiller can provide the needed cooling capacity and ESC uses three manipulated variables (CTA, CWF of the operating chiller, and CHWST setpoint). Three step tests are performed with CWF fixed at 10 kg/s and the CHWST setpoint fixed at 7 °C, while the CTA (ESC1) undergoes a 0.5 kg/s step change from 5, 6, and 10 kg/s, respectively. Based on the normalized step responses in Fig. 4, the input dynamics are estimated as:

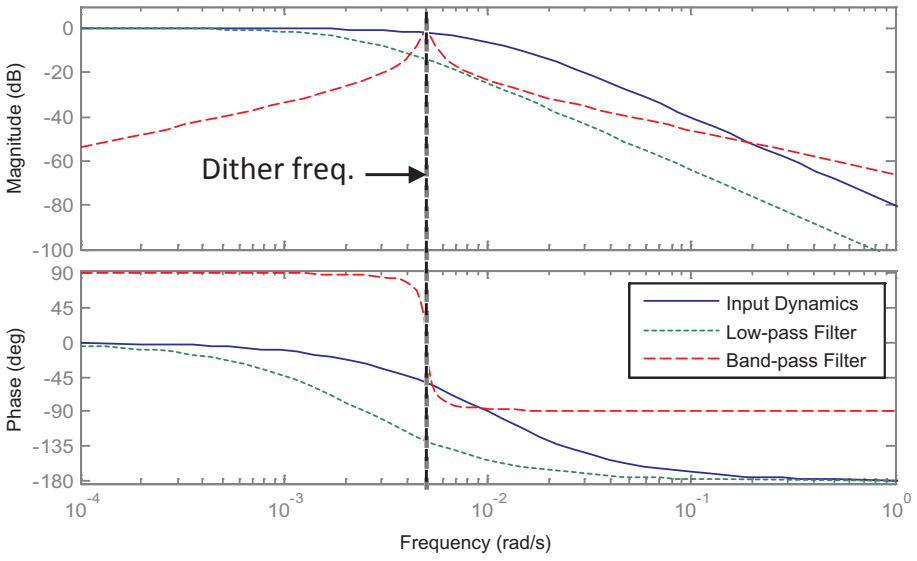

Fig. 5. Cooling tower air flow channel: selection of dither frequency, BP and LP filters.

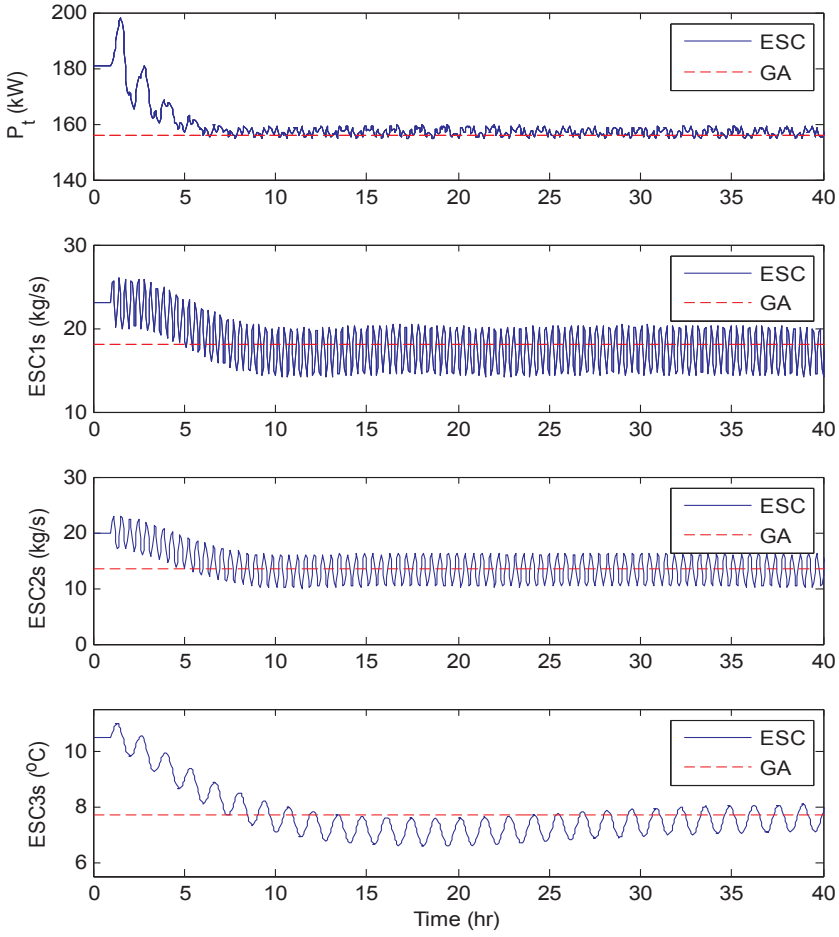

Fig. 6. ESC input and output trajectories for Case #1.

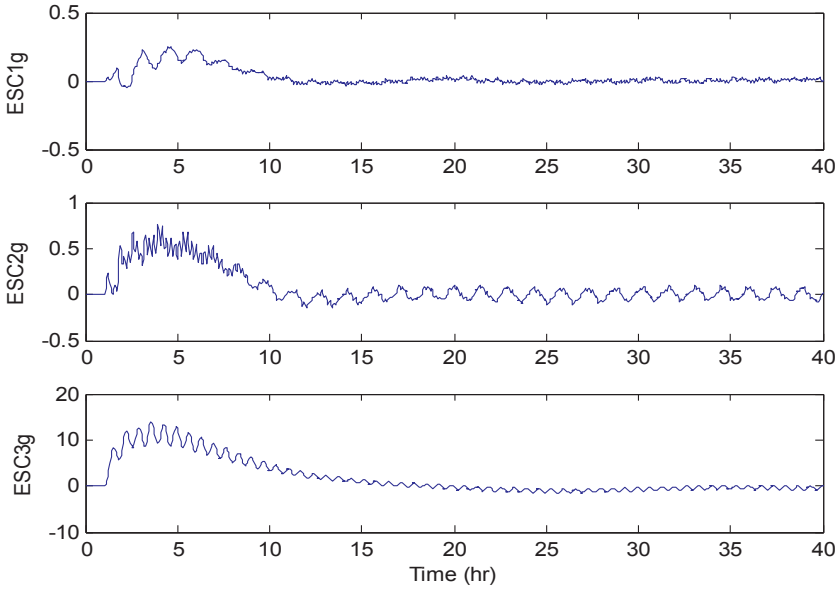

Fig. 7. Gradient trajectories for Case #1.

$$\hat{F}_A(s) = \frac{0.001^2}{s^2 + 2 \times 0.001s + 0.001^2} \tag{12}$$

Based on the ESC design guidelines proposed in [30], the dither frequency and amplitude are selected as 0.005 rad/s and 0.5 kg/s, respectively. As shown in Fig. 5, a 2nd-order band-pass filter is designed with the bandwidth from 0.0045 to 0.0055 rad/s. A 2nd-order low-pass filter is designed with the cut-off frequency of 0.0025 rad/s. The phase compensation between dither and demodulation is 0.92 rad. Similar step tests are performed for the ESC condenser water channel (ESC2) and the CHWST setpoint channel (ESC3) to determine the dither and demodulation signals, BP filters and LP filters. The ESC manipulated variables for these two channels are CWF and CHWST setpoint, respectively. Six different cases are used to evaluate the performance of the ESC optimization strategy and these cases are described next.

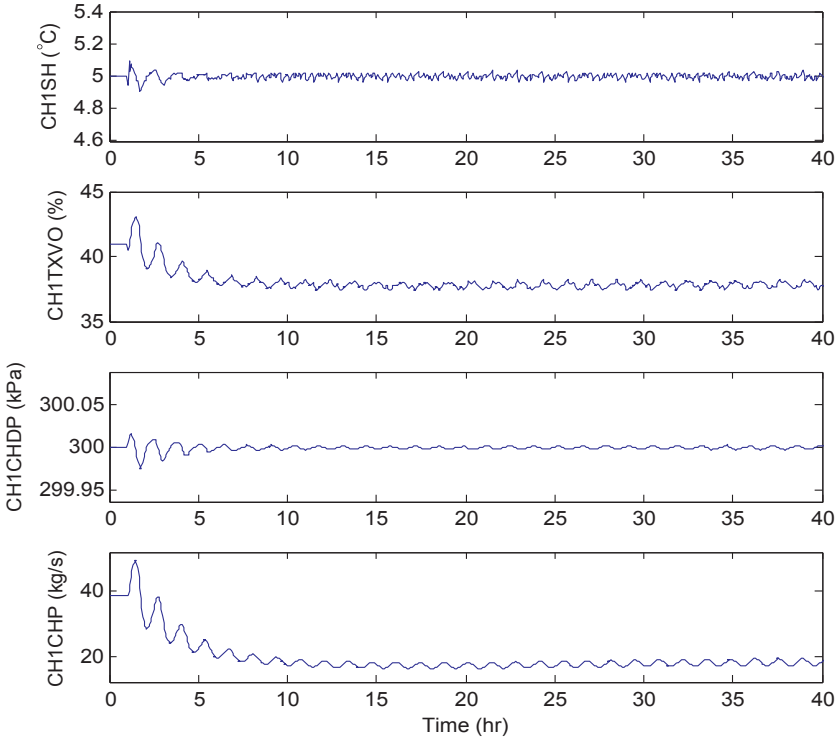

Fig. 8. Profiles of Chiller #1 SH, TXVO, CHDP and CHP for Case #1.

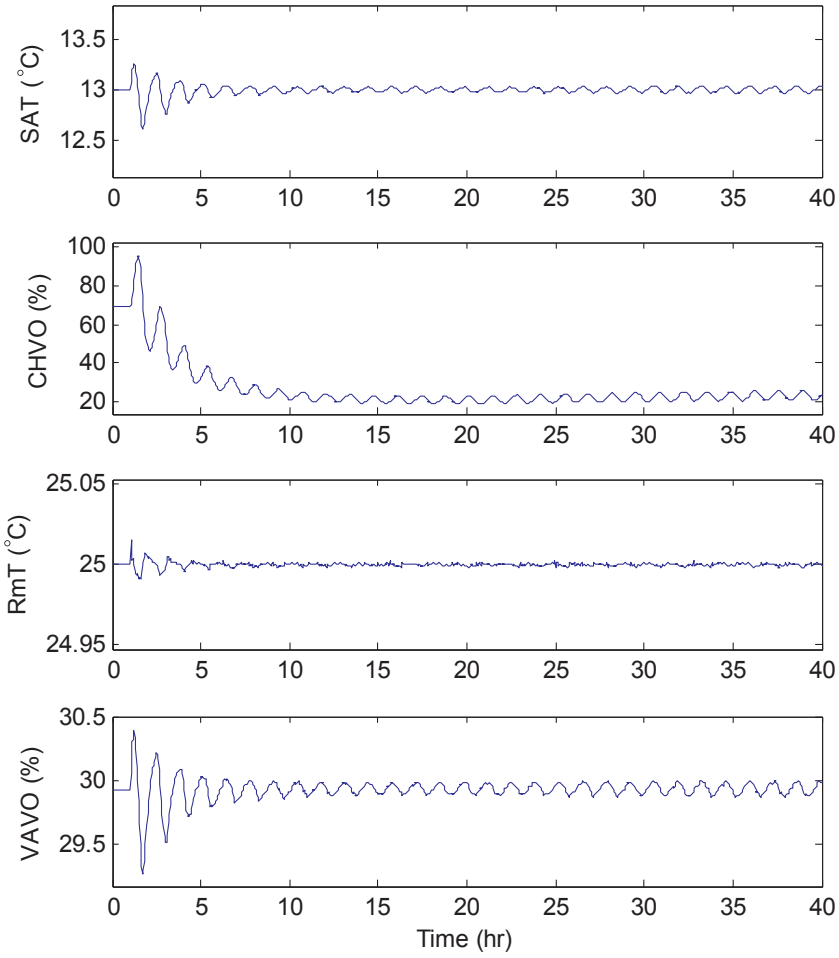

Fig. 9. Trajectories of SAT, CHVO (%), RmT and VAVO (%) for Case #1.

Table 2
ESC controller parameters for two-chiller ESC.

Parameter	ESC1 (CTA)	ESC2 (CH1CWF)	ESC3 (CHWST)	ESC4 (CH2CWF)
Dither freq. (rad/s)	0.005	0.0038	0.0013	0.0023
Dither amp.	3 kg/s	3 kg/s	0.5 °C	3 kg/s
Demodulation amp.	2/3 kg/s	2/3 kg/s	4 °C	2/3 kg/s
Demodulation phase (rad)	0.92	0.97	1.01	0.89
ω_{BPL} (rad/s)	0.0045	0.0034	0.0012	0.0021
ω_{BPH} (rad/s)	0.0055	0.0042	0.0014	0.0025
ω_{LP} (rad/s)	0.0025	0.0019	0.00615	0.00125
Integrator gain	0.0016	0.0052	0.00011	0.0006
Input range	[5, 55] kg/s	[5, 40] kg/s	[2, 11] °C	[5, 40] kg/s

5.1. Case #1: Single-chiller ESC

Single-chiller operation occurs when the cooling load can be met by the capacity of one chiller. In Case #1, single-chiller operation is simulated for Chiller #1 (CH1) with ambient conditions of 27 °C and 60% RH and heat gain of 250 kW. Optimization is achieved by ESC using three manipulated variables. Table 1 summarizes the ESC parameters for the simulation. The input and output trajectories for a 40 h simulation are shown in Fig. 6. The initial condition is set up as follows: CTA is 23 kg/s, CWF is 20 kg/s and the CHWST setpoint is 10.5 °C. ESC is turned on at $t = 1$ h and achieves an average steady-state total power of 157.2 kW, with a CTA command (**ESC1s**, where 's' stands for signal) of 17.2 kg/s, a CH1CWF command (**ESC2s**) of 13.4 kg/s, and a CHWST setpoint command (**ESC3s**) of 7.4 °C. The 2% settling time for total power is about 4.45 h. At steady state, ESC has reduced the power P_t from 180.9 kW to 157.1 kW, i.e. by 13.16%, from the initial condition.

The gradient trajectories of the input channels are plotted as ESC1g, ESC2g and ESC3g in Fig. 7, where it can be seen that all oscillate about 0 in steady state indicating the convergence of ESC to an interior optimum. Figs. 8 and 9 show the trajectories of regulated and manipulated variables of the inner-loop controls including SH, TXVO, CHDP and CHP for Chiller #1, and air-side variables SAT, CHVO (%), RmT and VAVO (%). SH, CHDP, SAT, and RmT are regulated well to their respective setpoints of 5 °C, 300kPa, 13 °C and 25 °C, which indicates that the power savings are achieved while maintaining the equipment and room at desired operating conditions.

To verify the steady-state performance of the ESC strategy, the

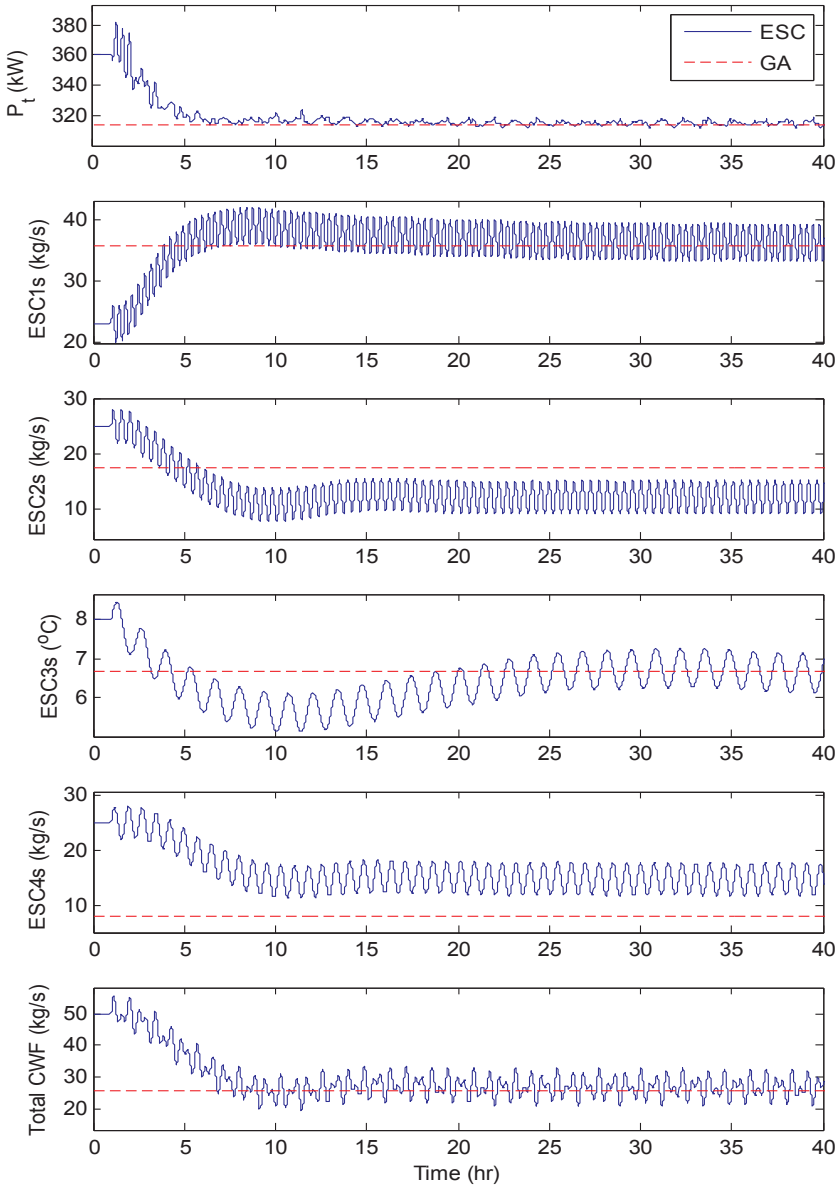

Fig. 10. ESC input and output trajectories for Case #2.

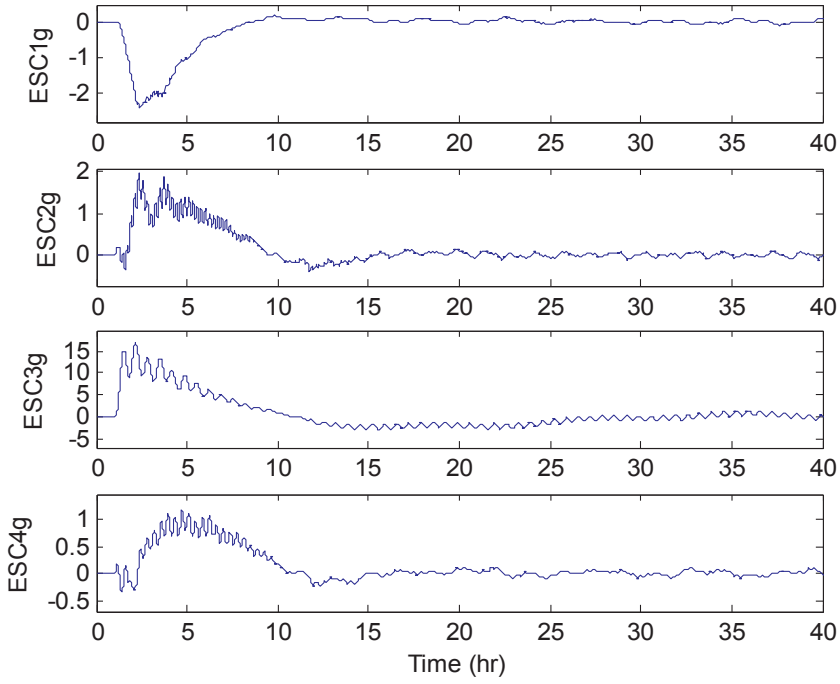

Fig. 11. Gradient trajectories for Case #2.

optimum is determined using global optimization algorithms such as genetic algorithm (GA) and Simplex that are available in the Dymola Optimization Library [41]. While not suitable for real-time optimization, such optimization procedures are effective for verification in simulation based studies as in this paper. The GA finds the global minimum total power to be 155.94 kW, corresponding to optimum values of CTA of 17.99 kg/s, CH1CWF of 13.50 kg/s, and CHWST setpoint of 7.70 °C, respectively. The ESC results for the total power, CTA, CWF and CHWST setpoint are close to the GA optimum with steady-state errors of 0.81%, 4.39%, 0.74% and 3.9%, respectively. For comparison, the GA results are included with the ESC input and output trajectories in Fig. 6.

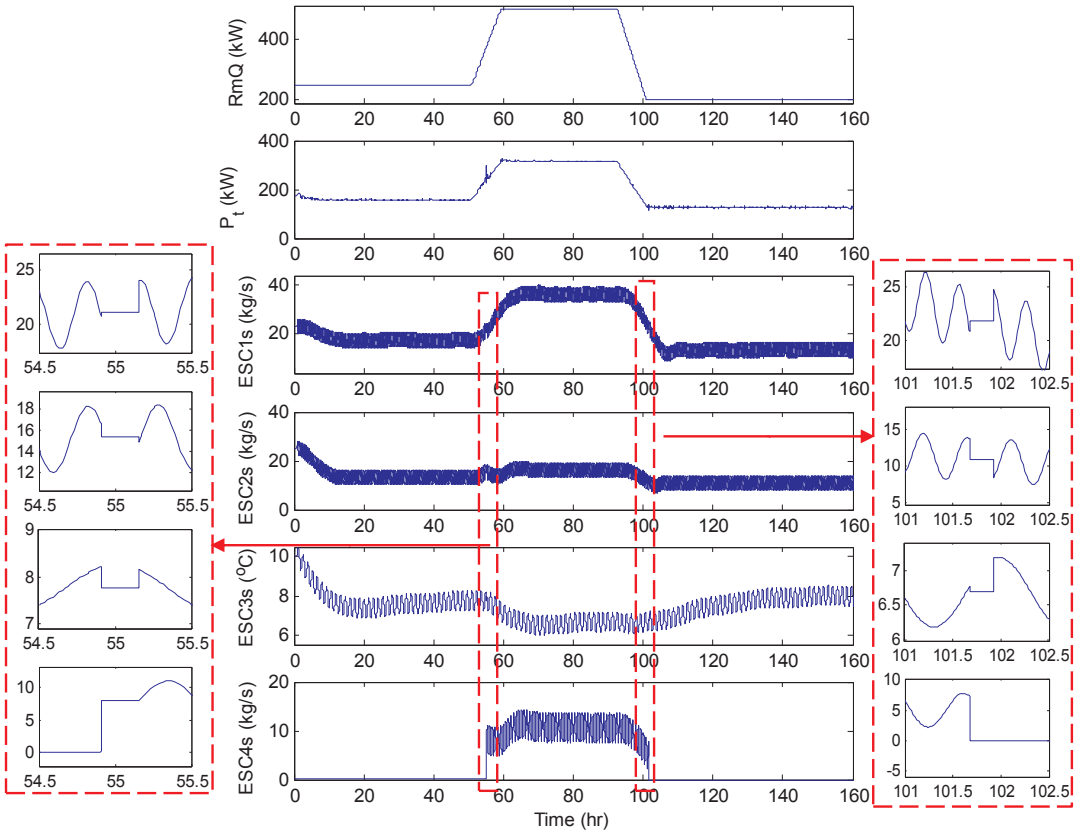

Fig. 12. Internal heat gain, input and output trajectories of ESC for Case #3.

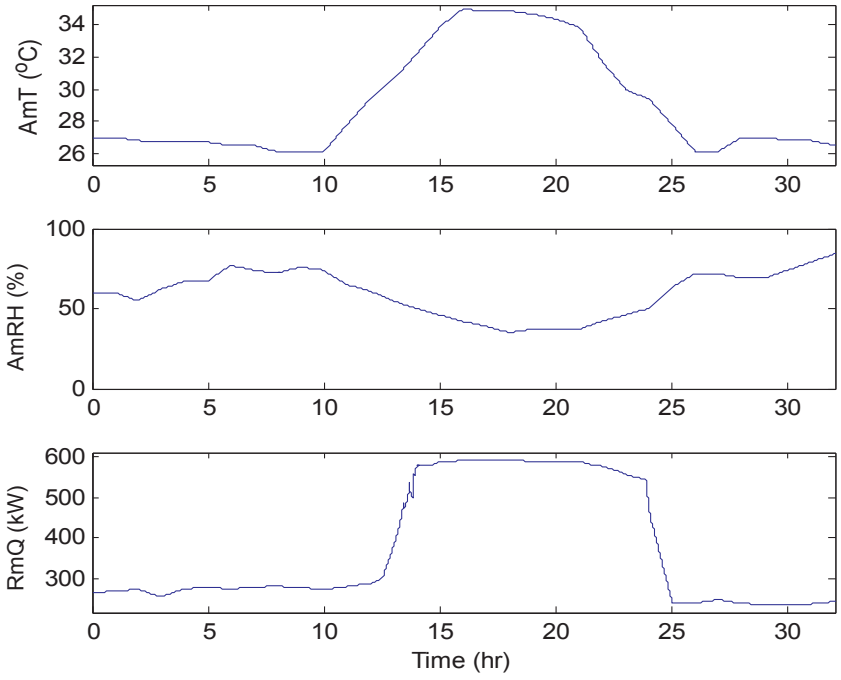

Fig. 13. Trajectories of ambient temperature, RH and internal heat gain for Case #4.

5.2. Case #2: Two-chiller ESC under fixed ambient and load conditions

For Case #2, the internal heat gain is increased to 500 kW and the ambient conditions are the same as Case #1. As one chiller cannot satisfy this cooling load, both chillers are turned on, which results in a four-input ESC scenario. For the CH2 condenser water flow channel, the input dynamics were estimated by following the step test procedure described previously. The ESC output signal for this channel is CH2CWF. The design parameters for the four-input ESC are listed in Table 2. Again, to evaluate the performance of the proposed ESC scheme, a GA is used to determine the global optimum. The GA found the minimum total power of 313.86 kW corresponding to optimal values of CTA of 35.70 kg/s, CH1CWF of 17.46 kg/s, CHWST setpoint of 6.69 °C, and CH2CWF of 8.04 kg/s, respectively. The total CWF is 25.5 kg/s (CH1CWF + CH2CWF). Optimum values determined by the GA are plotted in Fig. 10.

The input and output trajectories for the four-input ESC are also shown in Fig. 10. The simulation is initialized with the following values: CTA (**ESC1s**) is 23 kg/s, CH1CWF (**ESC2s**) is 25 kg/s, CHWST setpoint (**ESC3s**) is 8 °C, and CH2CWF (**ESC4s**) is 25 kg/s. ESC is turned

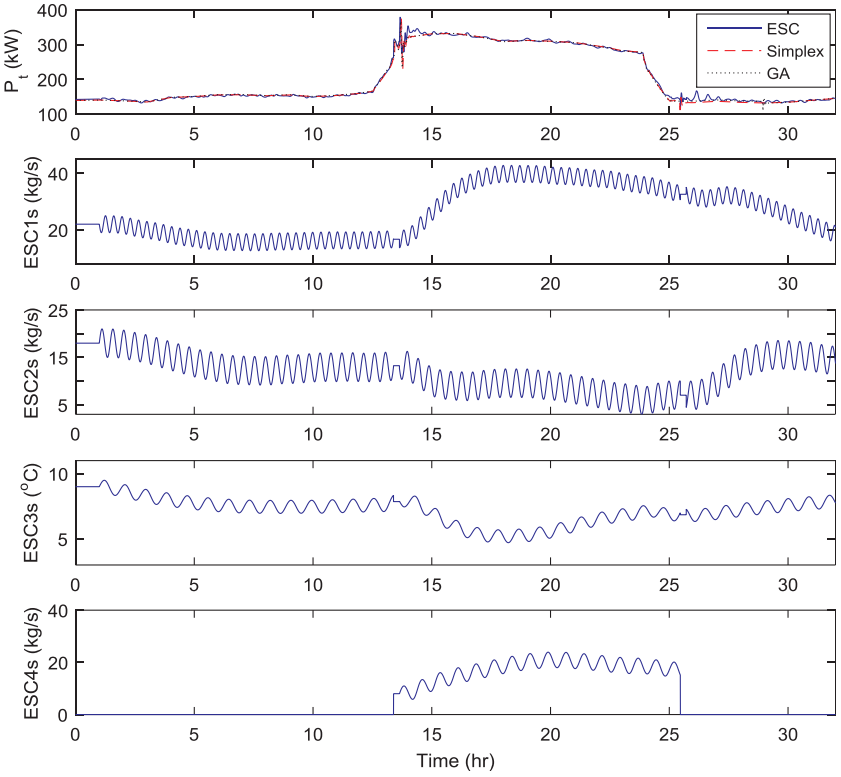

Fig. 14. Input and output trajectories of ESC for Case #4.

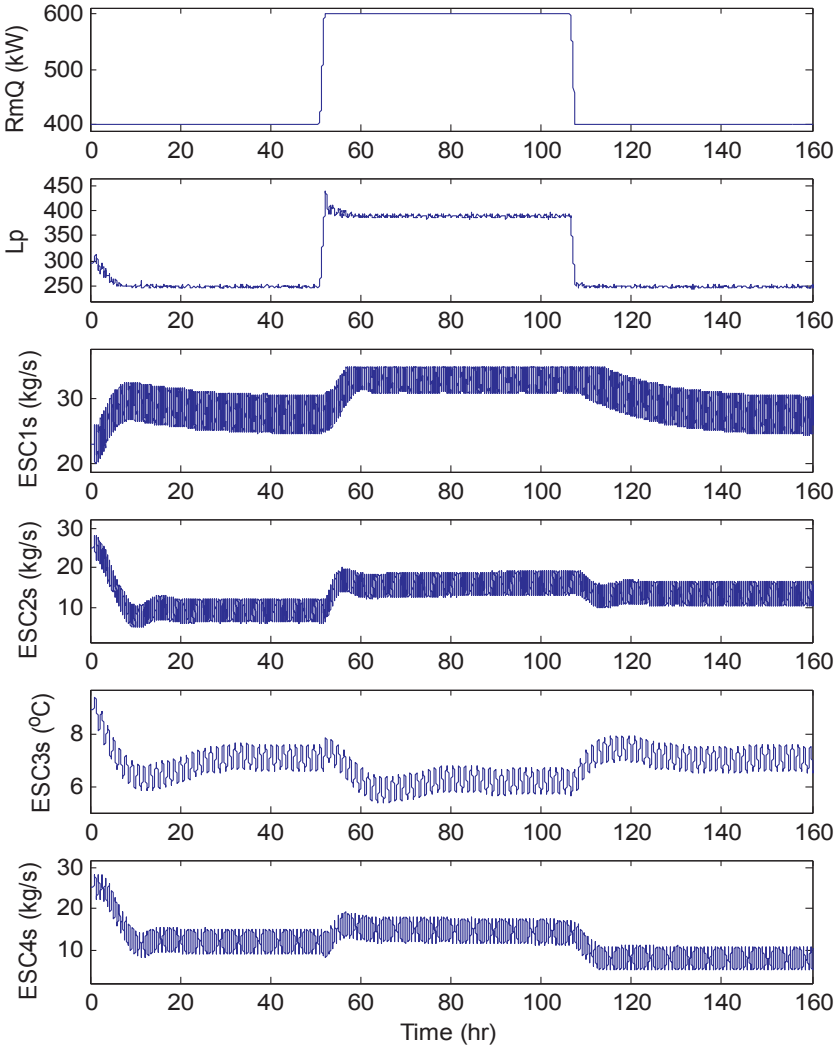

Fig. 15. Internal heat gain, input and output trajectories for Case #5.

on at $t = 1$ h and achieves an average steady-state total power of 314.7 kW with CTA = 36.41 kg/s, CH1CWF = 12.07 kg/s, CHWST setpoint = 6.67 °C, and CH2CWF = 14.36 kg/s. The total condensing water flow rate is 26.43 kg/s (i.e. CH1CWF + CH2CWF). The plant power consumption was reduced from 360.1 to 314.7 kW, i.e. by 12.6%. The steady-state error in power consumption between ESC and the GA is 0.27%. The 2% settling time for total power is approximately 4.72 h. Fig. 11 shows the gradient trajectories for the ESC manipulated variables. These plots indicate convergence to an interior optimum with all gradients oscillating around 0 at steady state.

At steady state, the errors between the ESC and GA results for CTA, CH1CWF, CHWST setpoint, and CH2CWF are 1.99%, 30.9%, 0.3% and 78.6%, respectively. Although the condensing water flow rates of the two chillers deviate significantly from the respective GA optimum, the total condensing water flow for ESC and GA have a steady-state error of only 3.65%.

5.3. Case #3: Chiller sequencing under variable load and fixed ambient condition

Case #3 presents a scenario with a variable load and the same ambient conditions as in Cases #1 and #2. As shown in Fig. 12, beginning at $t = 51$ h, the internal heat gain is increased at a rate of 0.5 kW/min from 250 kW to 500 kW. Then, at $t = 92.4$ h, the internal heat gain is decreased at a rate of 0.6 kW/min from 500 kW to 200 kW. This scenario requires the operation of one chiller at the lower load conditions and two chillers at the higher load, thus the sequencing strategy described in [30] is used to turn on and off CH2 and associated pumps as necessary. The simulation is started with CTA = 23 kg/s, CH1CWF = 25 kg/s, and CHWST setpoint = 10 °C.

The three-input ESC for CH1 is turned on at $t = 1$ h, and converges to an average steady-state total power of 156.9 kW under the load of 250 kW. The corresponding optimal values of the ESC variables are CTA = 17.2 kg/s, CH1CWF = 13.2 kg/s, and CHWST setpoint = 7.56 °C. With the increasing load starting at $t = 51$ h, CH2 is engaged at $t = 54.91$ h when the chilled water valve opening exceeds 90% for 5 min. The ESC signals for CH1 are frozen at their previous values during the 15-min startup period of CH2. The four-input-ESC for two-chiller operation is engaged after the startup period is over. A magnified view of these variables prior to, during, and immediately after the startup period is shown on the left side of Fig. 12.

During the period with the load of 500 kW, an average steady-state total power of 316.2 kW is obtained with average values of CTA = 36.7 kg/s, CH1CWF = 16.7 kg/s, CHWST setpoint = 6.6 °C, and CH2CWF = 10.1 kg/s. At $t = 92.4$ h, the load begins decreasing and at $t = 101.7$ h, CH2 is turned off when the CH2 compressor speed drops below 30% of its maximum for 5 min. The 15-min shutdown process is carried out after freezing the three ESC signals used when only one chiller is in operation. The fourth ESC signal corresponding to the CH2CWF decreases to 0 when the second chiller is turned off. A magnified view of the four ESC variables prior to, during, and immediately after the shutdown period is shown on the right side of Fig. 12.

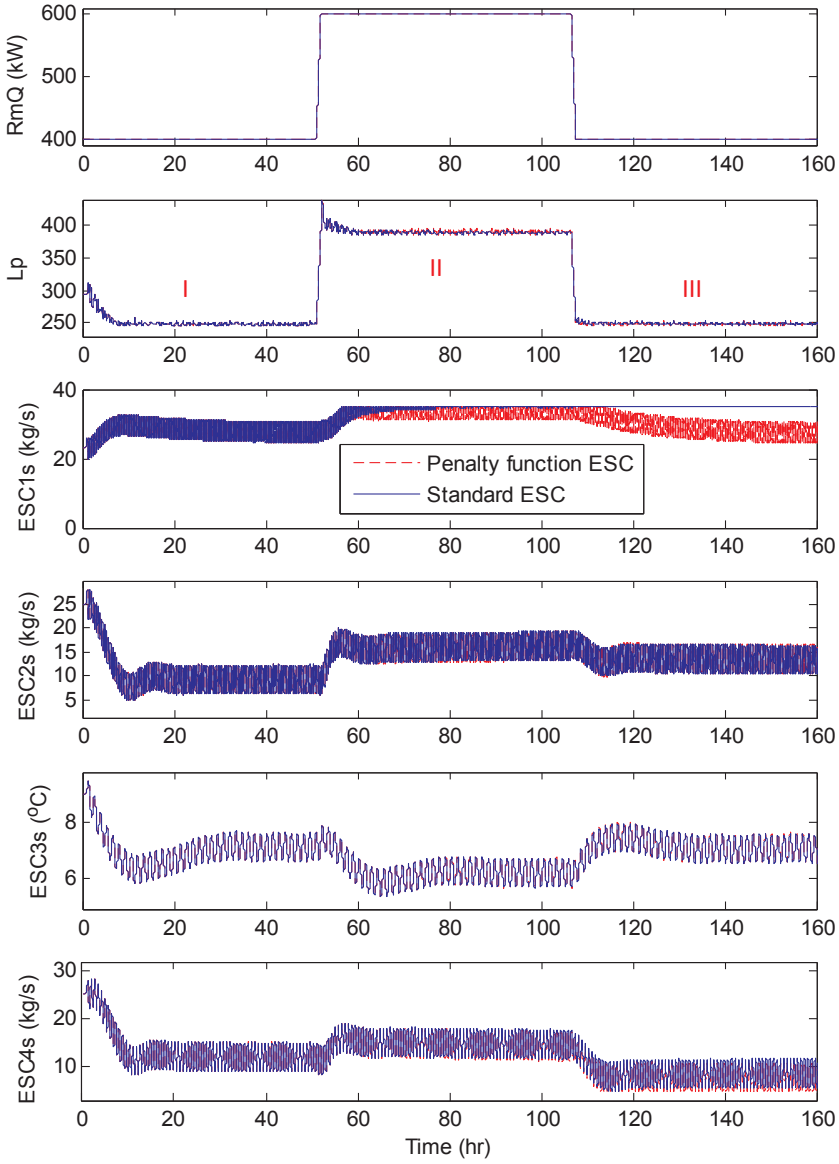

Fig. 16. Input and output trajectories for Case #5.

Under the cooling load of 200 kW, an average steady-state total power of 126.3 kW is obtained with CTA = 13.5 kg/s, CH1CWF = 10.5 kg/s, and CHWST setpoint = 7.9 °C. Although not shown, the gradient trajectories indicate that ESC converges to a steady-state optimum under the three different load conditions.

5.4. Case #4: Chiller sequencing with realistic ambient and load profiles

Case #4 considers a scenario with time-varying ambient conditions and cooling load. Fig. 13 shows a 32-h profile for ambient temperature and relative humidity for the Dallas-Fort Worth area obtained from the TMY2 database [42]. Also shown in Fig. 13 is the internal heat gain profile used for this case. The simulation is started with CTA = 22 kg/s, CH1CWF = 18 kg/s, and CHWST setpoint = 9 °C.

The ESC input and output trajectories for Case #4 are shown in Fig. 14. The three-input ESC is turned on at t = 1 h. In response to the variation of ambient conditions and internal heat gain, CH2 is turned on at t = 13.39 h and turned off at t = 25.49 h. The ESC inputs demonstrate time-varying input trajectories with the averaged power of 205.56 kW. To evaluate the performance of the proposed ESC sequencing strategy, the benchmark case is set with a constant-input operation which is optimized by running through the whole 32-h simulation period using the aforementioned procedure of simulation based optimization. Both Simplex and GA in Dymola are used to find the fixed inputs that minimize the average power consumption throughout the 32-h simulation period. The Simplex and GA method error tolerances are 0.001.

The Simplex method converges to 24.47 kg/s for CTA, 13.15 kg/s for CH1CWF, 7.27 °C for CHWST setpoint and 10.73 kg/s for CH2CWF, resulting in the average power consumption of 203.98 kW. The GA method converges to 24.34 kg/s for CTA, 11.58 kg/s for CH1CWF, 7.08 °C for CHWST setpoint and 10.53 kg/s for CH2CWF, resulting in the average power of 204.54 kW. The ESC strategy shows higher power consumption than the GA and Simplex methods during the transitional periods (t = 12–15 h and 24–27.5 h), while its power consumption is lower for other periods of approximate steady state.

5.5. Case #5: Penalty function based ESC

Case #5 examines the impact of input saturation on the ESC strategy by limiting CTA to a maximum value of 35 kg/s. Throughout the simulation the ambient conditions are maintained at 27 °C and 60%RH. The internal heat gain, shown in the top panel of Fig. 15, is initially 400 kW, and then beginning at t = 51 h, increases linearly over a 1-h

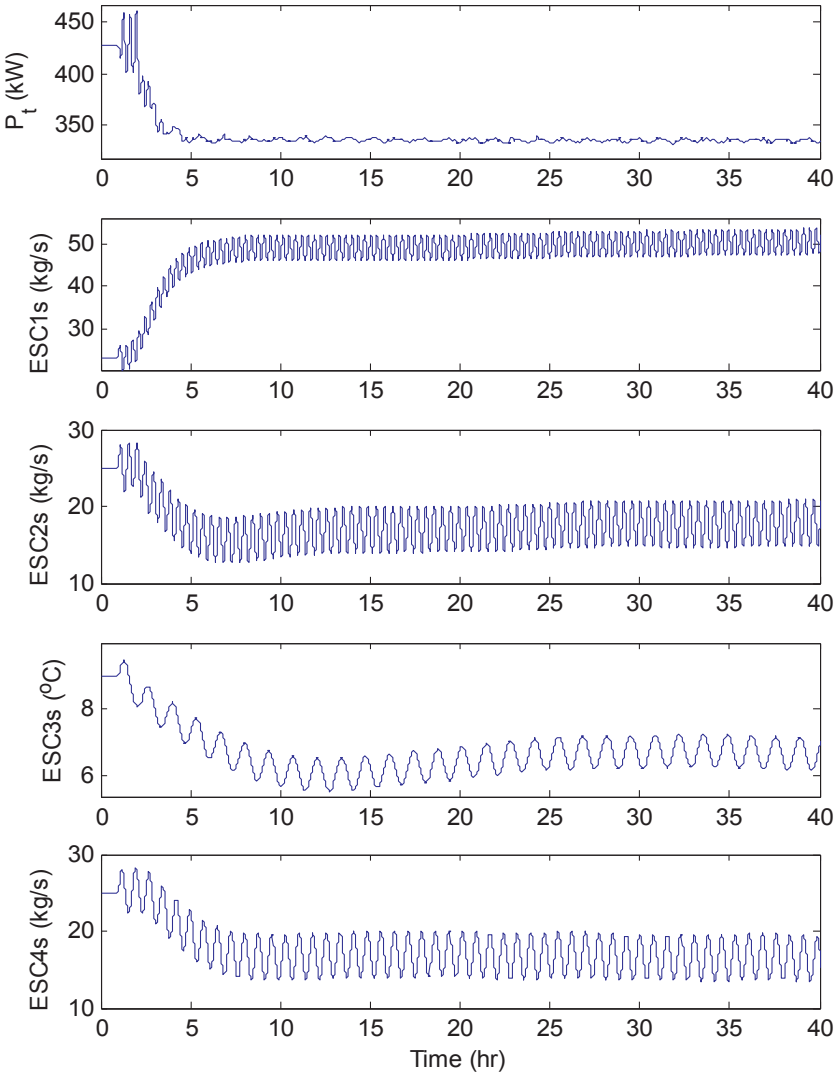

Fig. 17. Input and output trajectories of ESC under 40% refrigerant charge for CH2.

period to 600 kW. Beginning at $t = 106.6$ h, the heat gain decreases linearly over a 1-h period to 400 kW. The performance index for ESC is the combination of the total power and input-saturation induced penalty terms. The weight of the penalty term for the cooling tower air flow channel is $\gamma_{CTA} = 1.1$.

The input and output trajectories in Fig. 15 show that ESC converges during the period of the first load of 400 kW to average values of CTA = 27.89 kg/s, CH1CWF = 8.9 kg/s, CHWST setpoint = 7.1 °C and CH2CWF = 12.6 kg/s. With the load increased to 600 kW, CTA saturates at its upper limit of 35 kg/s while CH1CWF, CH2CWF, and CHWST setpoint settle to 15.51 kg/s, 14.3 kg/s and 6.2 °C, respectively. When the load returns to 400 kW, ESC converges with CTA = 27.35 kg/s, CH1CWF = 13.9 kg/s, CHWST setpoint = 6.9 °C and CH2CWF = 7.7 kg/s.

Fig. 16 shows the same case simulated without the penalty for input saturation in the ESC feedback. For ease of discussion, this benchmark result is referred to as "standard ESC". At the 600 kW load (i.e., identified as period II in Fig. 16), CTA is saturated at its upper limit of 35 kg/s. With standard ESC, CTA is stuck at this limit (i.e. integral windup) and unable to track the new optimum corresponding to the 400 kW load. This occurs because during Period II, the integrator in ESC continues to increase in an effort to drive CTA to an optimum value beyond its upper limit. When the conditions change and the optimum moves to a value between the upper and lower limits, ESC is unable to drive CTA away from the upper limit due to the persistence of this large integral error. By contrast, the penalty-function based anti-windup ESC avoids this undesirable situation by imposing a penalty for values of CTA above the upper limit.

It is noteworthy that both methods have the same steady-state average power consumption of 248.4 kW for Period I. The steady-state average power consumption for Period II is 390.7 kW with the penalty-function based ESC and 388.7 kW with standard ESC. The steady-state average power consumption for Period III is 248.1 kW with the penalty-function based ESC and 249.8 kW with standard ESC. For Period II, penalty-function based ESC results in a higher power consumption than that by standard ESC. During this period the optimal CTA is greater than 35 kg/s and standard ESC results in CTA = 35 kg/s, which is the upper limit of that channel, while the penalty-function based ESC results in a CTA oscillating below the upper limit. For Period III, the penalty-function based ESC searches for an optimal CTA that achieves a smaller power consumption while standard ESC is stuck at 35 kg/s. The differences in performance described here are modest in terms of average power; however, this example demonstrates an important capability that penalty-function based ESC provides.

5.6. Case #6: ESC for efficiency recovery in degraded chillers

In practice, a major cause for suboptimal operation of HVAC systems is equipment degradation. For chiller plants, equipment degradations may include heat exchanger fouling, low refrigerant charge,

cooling tower fill deposits, wear, debris accumulation (fouling) and leakage of compressor. Online fault detection and diagnostics (FDD) of these types of problems, in spite of significant development in the past, is not common. Also, degradation from faults can persist for long periods of time before becoming sufficiently large to be noticed, and even then immediate maintenance may not occur. Under such circumstances, the goal is to operate the plant at the maximum achievable plant efficiency. Plant recalibration as required by model-based control methods is time-consuming and expensive. In comparison, ESC will continue to optimize system operation in the presence of equipment degradation, thus bringing the benefit of efficiency recovery. Case #6 evaluates this for a low refrigerant charge fault.

The ambient conditions and internal heat gain for Case #6 are same as those in Case #2. CH1 is fully charged while CH2 has a 40% charge (i.e., it has 60% less refrigerant than normal). As shown in Fig. 17, the simulation starts with CTA = 23 kg/s, CH1CWF = 25 kg/s, CHWST setpoint = 9 °C, and CH2CWF = 25 kg/s. ESC is turned on at t = 1 h and results in an average steady-state total power of 341.2 kW with optimal CTA = 50.74 kg/s, CH1CWF = 17.64 kg/s, CHWST setpoint = 6.65 °C, and CH2CWF = 16.65 kg/s.

The optimum power achieved by ESC in the presence of the fault is 8.2% higher than the 315.5 kW achieved by ESC when both chillers are fully charged (Case #2). If, however, the plant is operated in the presence of the fault using the optimum values determined when both chillers are fully charged, the resultant average total power consumption is 362.4 kW, a value that is 5.85% higher than that achievable by ESC. This case demonstrates that the plant power consumption is increased by an under-charged chiller, and that ESC is able to determine optimum input settings that maximize the achievable efficiency in the presence of this fault.

6. Conclusions

A real-time optimization strategy using penalty-function based multivariate ESC is proposed for minimizing the total power consumption of a chilled water plant with chillers in parallel. The ESC can optimize the cooling tower air flow rate, condenser water flow rate and leaving chiller water temperature setpoint simultaneously. The proposed strategy is simulated with a Modelica based dynamic simulation model of a chilled-water plant with two chillers in parallel. Case studies have been carried out for single-chiller and two-chiller operation, under fixed and time-varying ambient and load conditions. For the simulated operational scenarios, the proposed strategy demonstrates the capability of convergence to a close proximity of the calibrated optimum under fixed and varied ambient and load conditions. An illustrative simulation case demonstrated that the penalty function based ESC can handle the integral windup due to input constraints. Also, the simulation for the scenario of refrigerant under-charge shows that the proposed ESC strategy can realize energy efficiency recovery under equipment degradation.

Appendix A

See Tables A1 and A2.

Table A1
Design specifications of chiller evaporator and condenser.

Parameters	Refrigerant	Tube length (m)	Tube inner diameter (m)	Number of parallel tubes	Tube material
Evaporator	R134a	5	0.01960	149	Copper
Condenser	R134a	5	0.01606	149	Copper

Table A2
Design specifications of compressor.

Parameters	Displacement (m^3)	Volumetric efficiency (%)	Isentropic efficiency (%)
Cooling coil	0.0034	85	80

References

[1] U.S. Department of Energy. Buildings energy data book < http://web.archive.org/web/20130214024505/http:/buildingsdatabook.eren.doe.gov/ChapterIntro1.aspx > .
[2] U.S. Department of Energy. Energy efficiency trends in residential and commercial buildings; 2008. p. 1–32.
[3] Yu FW, Chan KT. Optimization of water-cooled chiller system with load-based speed control. Appl Energy 2008;85(10):931–50.
[4] Benton DJ, Hydeman M, Bowman CF, Miller P. An improved cooling tower algorithm for the CoolTools™ simulation model. ASHRAE Trans 2002;108(1) [Paper #AC-02-9-4].
[5] Hydeman M, Zhou G. Optimizing chilled water plant control. ASHRAE J 2007:45–54.
[6] Ahn BC, Mitchell JW. Optimal control development for chilled water plants using a quadratic representation. Energy Build 2001;33:371–8.
[7] Gordon JM, Ng KC, Chua HT. Centrifugal chillers: thermodynamic modelling and a diagnostic case study. Int J Refrig 1995;18(4):253–7.
[8] Powell KM, Cole WJ, Ekarika UF, Edgar TF. Dynamic optimization of a campus cooling system with thermal storage. In: Proceedings of the 2013 European control conference. Zürich (Switzerland); 2013. p. 4077–82.
[9] Olson RT, Liebman JS. Optimization of a chilled water plant using sequential quadratic programming. Eng Optim 1990;15(30):171–91.
[10] Kusiak A, Li M, Tang F. Modeling and optimization of HVAC energy consumption. Appl Energy 2010;87(10):3092–102.
[11] Huang S, Zuo W, Sohn MD. Amelioration of the cooling load based chiller sequencing control. Appl Energy 2016;168:204–15.
[12] Deng K, Sun Y, Li S, Lu Y, Brouwer J, Mehta PG, Zhou MC, Chakratorty A. Model predictive control of central chiller plant with thermal energy storage via dynamic programming and mixed-integer linear programming. IEEE Trans Autom Sci Eng 2014:1–14.
[13] Zhu J, Yang Q, Lu J. Model predictive control of chilled water temperature for centralized HVAC systems. In: Proceedings of the 2013 IEEE electrical power & energy conference; 2013 [5 pages].
[14] Chow TT, Zhang GQ, Lin Z, Song CL. Global optimization of absorption chiller system by genetic algorithm and neural network. Energy Build 2002;34(1):103–9.
[15] Chang YC, Lin JK, Chuang MH. Optimal chiller loading by genetic algorithm for reducing energy consumption. Energy Build 2005;37(2):147–55.
[16] Ma Z, Wang S. Supervisory and optimal control of central chiller plants using simplified adaptive models and genetic algorithm. Appl Energy 2011;88(1):198–211.
[17] Lee W, Lin L. Optimal chiller loading by particle swarm algorithm for reducing energy consumption. Appl Energy 2009;29(8–9):1730–4.
[18] Ardakani AJ, Ardakani FF, Hosseinian SH. A novel approach for optimal chiller loading using particle swarm optimization. Energy Build 2008;40(12):2177–87.

[19] Ariyur KB, Krstić M. Real time optimization by extremum seeking control. Hoboken (NJ): Wiley; 2003.
[20] Li P, Li Y, Seem JE. Efficient operation of air-side economizer using extremum seeking control. ASME J Dyn Syst, Measur, Control 2010;132(3):031009. [10 pages].
[21] Mu B, Li Y, House JM, Salsbury TI. Experimental evaluation of extremum seeking control for efficient operation of airside economizers. Control Eng Pract April 2016;50:37–47.
[22] Burns D, Laughman C. Extremum seeking control for energy optimization of vapor compression systems. In: Purdue compressor engineering, refrigeration & air conditioning & high performance buildings conference. West Lafayette (IN, USA); 2012 [8 pages].
[23] Xiao Y, Li Y, Seem JE, Dong L. Multi-variable extremum seeking control for mini-split air-conditioning system. In: Purdue compressor engineering, refrigeration and air conditioning and high performance buildings conference. West Lafayette (IN, USA); 2014 [12 pages].
[24] Dong L, Li Y, Mu B, Xiao Y. Self-optimizing control of air-source heat pump with multivariable extremum seeking. Appl Thermal Eng 2014;84(5):180–95.
[25] Hu B, Li Y, Mu B, Wang S, Seem JE, Cao F. Extremum seeking control for efficient operation of hybrid ground source heat pump system. Renew Energy 2016;86:332–46.
[26] Sane HS, Haugstetter C, Bortoff SA. Building HVAC control systems - role of controls and optimization. In: Proceedings of American control conference. Minneapolis (MN, USA); 2006. p. 1121–6.
[27] Li X, Li Y, Seem JE. Dynamic modeling and self-optimizing operation of chilled water systems using extremum seeking control. Energy Build 2013;58:172–82.
[28] Mu B, Li Y, Seem JE. Comparison of several self-optimizing control methods for efficient operation for a chilled water plant. In: Proceedings of 2013 ASME dynamic systems and control conference, Paper No. DSCC2013-4097. Palo Alto (CA); 2013.
[29] Mu B, Li Y, Seem JE, Hu B. A multi-variable newton-based extremum seeking control for condenser water loop optimization of chilled water plant. ASME J Dynam Syst, Measur Control 2015;137(11):111011. [10 pages].
[30] Mu B, Li Y, Salsbury TI, House JM. Extremum seeking based control strategy for a chilled-water plant with parallel chillers. In: Proceedings of 2015 ASME dynamic systems and control conference. Columbus (OH); 2015.
[31] Mu B, Li Y, Salsbury TI, House JM. Optimization and sequencing of chilled-water plant based on extremum seeking control. In: 2016 American control conference, July 6–8. Boston (MA); 2016.
[32] Krstić M, Wang H-H. Stability of extremum seeking feedback for general nonlinear dynamic systems. Automatica 2000;36:595–601.
[33] Krstić M. Performance improvement and limitations in extremum seeking control. Syst Control Lett 2000;39(5):313–26.
[34] Rotea MA. Analysis of multivariable extremum seeking algorithm. In: Proceedings of American control conference. Chicago (IL); 2000. p. 433–7.
[35] Tan Y, Li Y, Mareels I. Extremum seeking for constrained inputs. IEEE Trans Autom Control 2013;58(9):2405–10.
[36] Peng Y, Vrancic D, Hanus R. Anti-windup, bumpless and conditioned transfer techniques for PID controllers. IEEE Control Syst Mag 1993;16(4):48–57.
[37] Dassault Systems. Dymola; 2015 < http://www.3ds.com/products-services/catia/products/dymola > .
[38] TLK-Thermo. GmbH. TIL Suite < http://www.tlk-thermo.com/en/software-products/til.html > .
[39] Richter CC. Proposal of new object-oriented equation-based model libraries for thermodynamic systems Institute for Thermodynamics, Technical University at Braunschweig; 2008. Ph.D. Thesis.
[40] AHRI Standard 550/590 (I-P). Standard for performance rating of water-chilling and heat pump water-heating packages using the vapor compressor cycle. Air-Conditioning, Heating & Refrigeration Institute; 2011.
[41] DLR Institute of Robotics and Mechatronics. Optimization library; 2015.
[42] National Solar Radiation Data Base. 1961–1990: typical meteorological year 2 < http://rredc.nrel.gov/solar/old_data/nsrdb/1961-1990/tmy2/ > .